Agricultural Water Management 295 (2024) 108773

Contents lists available at ScienceDirect

Agricultural Water Management

journal homepage: www.elsevier.com/locate/agwat

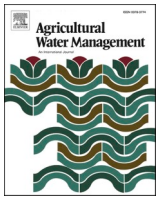

Benefits and pitfalls of irrigation timing and water amounts derived from satellite soil moisture

Luca Zappa [a,*], Jacopo Dari [b,c], Sara Modanesi [c], Raphael Quast [a], Luca Brocca [c], Gabrielle De Lannoy [d], Christian Massari [c], Pere Quintana-Seguí [e], Anais Barella-Ortiz [e], Wouter Dorigo [a]

[a] Department of Geodesy and Geoinformation, TU Wien, Vienna 1040, Austria
[b] Department of Civil and Environmental Engineering, University of Perugia, via G. Duranti 93, Perugia 06125, Italy
[c] National Research Council, Research Institute for Geo-Hydrological Protection, via Madonna Alta, Perugia 06128, Italy
[d] Department of Earth and Environmental Sciences, KU Leuven, Celestijnenlaan 200E, Heverlee 3001, Belgium
[e] Ebro Observatory (OE), Ramon Llull University – CSIC, Carrer Observatori 3-A, Roquetes 43520, Spain

ARTICLE INFO

Handling Editor: J.E. Fernández

Keywords:
Irrigation
Intercomparison
Spatio-temporal analysis
Soil moisture
Sentinel-1

ABSTRACT

Despite the key role of irrigation in the Earth system, we lack fundamental information regarding the distribution of irrigated fields, irrigation timing and the amount of water utilized. In the past years, the SM_Delta and SM_Inversion approaches have been independently developed to provide estimates of irrigation timing and water amounts based on satellite soil moisture data. The SM_Delta approach retrieves irrigation from variations in soil moisture between an individual pixel and the surrounding rainfed area, while the SM_Inversion approach estimates the total amount of water entering the soil, then irrigation is derived by subtracting precipitation. In this study, we perform a comprehensive assessment of irrigation estimates from the SM_Delta and SM_Inversion algorithms based on Sentinel-1 surface soil moisture retrievals at 1 km resolution. Our analysis focuses on the Ebro basin, an irrigated region in Spain covering 83000 km^2, during the period 2017–2019. We assess the ability of the two methods to discriminate irrigated and rainfed pixels, then we quantify the agreement of irrigation timing and water volumes with reference irrigation data. An inter-comparison between estimates from the SM_Delta and SM_Inversion methods is carried out considering both temporal and spatial features, i.e., monthly irrigation peaks and spatial irrigation patterns. Finally, we explore two potential applications of satellite-derived irrigation estimates: attributing irrigation water volumes to specific irrigation systems and to individual crops. We observe that both methods erroneously retrieve irrigation over rainfed pixels, and are therefore not suitable to map irrigated and rainfed fields. However, when auxiliary information on irrigated fields is available, we find a satisfactory agreement between district-scale reference data and satellite-retrieved irrigation, using both the SM_Delta and SM_Inversion approaches (Pearson R equal to 0.67 and 0.71, bias equal to −4.99 and −4.75 mm/15 days, respectively). When aggregated in space or time, the irrigation estimates exhibit coherent temporal dynamics and spatial patterns. For instance, estimates from both SM_Delta and SM_Inversion capture the delayed irrigation that occurred in 2018 due to wetter than usual conditions in spring. However, at the pixel-scale, limited consistency exists between irrigation estimates from the two methods due to different assumptions and parameterizations, e.g., use of constant vs pixel-specific soil water capacity (in the SM_Delta and SM_Inversion, respectively). Overall, the study demonstrates the reliability of irrigation estimates derived from the SM_Delta and SM_Inversion approaches, especially when shifting from small spatial and short temporal scales (pixel level, sub-weekly) to larger and longer scales (district level, seasonal). Hence, satellite-based irrigation estimates could inform water resources managers and basin authorities, as well as serve the modelling community by providing reliable information on the timing and the amounts of water employed at the basin level.

* Corresponding author.
E-mail address: luca.zappa@geo.tuwien.ac.at (L. Zappa).

https://doi.org/10.1016/j.agwat.2024.108773
Received 4 October 2023; Received in revised form 12 February 2024; Accepted 9 March 2024
Available online 13 March 2024

1. Introduction

Sub-optimal water availability, especially during key phenological stages, is a main driver of crop yield losses in many regions of the world (Lobell et al., 2009; Vogel et al., 2019). Irrigated agriculture contributes to reducing such losses and can therefore enhance food security (Kukal and Irmak, 2019). In addition, irrigation enables to expand the climate-constrained suitability of certain regions for crop production. For instance, several semi-arid and arid locations have witnessed intense expansions of irrigation in the past decades, resulting in an overall increase of agricultural land area worldwide (Siebert et al., 2015).

Recent analysis estimated that irrigated agriculture delivers approximately 40% of the entire food production while covering roughly 20% of cropland (Unesco, 2019). Furthermore, irrigation is responsible for 70% of freshwater withdrawals, as a global average, while regionally the percentage varies considerably, reaching up to 90%, e.g., in the Middle East and South Asia (McDermid et al., 2023). Therefore, it is not surprising that irrigated agriculture is often associated with negative environmental phenomena, such as groundwater depletion, soil salinity, and nutrient leaching (Deng et al., 2018; Famiglietti, 2014; Pokhrel et al., 2016). Also, extensive irrigation can affect local and regional meteorological conditions, by feedbacks on temperature, humidity and precipitation (Cook et al., 2015; Pei et al., 2016).

Despite the pivotal role of irrigation in the Earth System (McDermid et al., 2023), little is known about the amount of water applied at field-to-farm level on regional-to-continental scales (Dorigo et al., 2021; Massari et al., 2021). Survey-based irrigation estimates, such as those from AQUASTAT (https://www.fao.org/aquastat/), are generally provided as lump yearly values at national level. Even without considering the large uncertainties in such estimates, due to, e.g., self-reporting of farmers, upscaling procedures, and representativeness of surveyed farms, their use is of limited value for many applications. For instance, water resource managers, national and regional authorities, and irrigation consortia require spatially explicit and temporally detailed information about water consumption for irrigation (Massari et al., 2021).

Various models, i.e., land surface, hydrological, and crop growth models, are increasingly including irrigation schemes to account for the impact of irrigation on the energy balance, the water cycle, and crop productivity (De Rosnay, 2003; Ozdogan et al., 2010; Pokhrel et al., 2012). However, irrigation estimates from such models rely on a number of assumptions and simplifications. For instance, in many models irrigation is triggered whenever modelled soil moisture drops below a certain threshold, and the amount of water applied re-establishes optimal soil moisture conditions (Massari et al., 2021). In reality, the decisions of farmers on when and how much to irrigate are often not physically-based but driven by factors, such as water turns and water regulations imposed by the irrigation consortia, and crop-specific subsidies, which cannot be represented in models. Even when the models contain more complex and advanced irrigation schemes, certain parameters need to be set a-priori. For example, irrigation efficiency is a key parameter often characterized by a static value depending on the irrigation system, with high efficiencies for drip irrigation and low efficiencies for surface methods (Puy et al., 2022a). Even assuming that the irrigation system is known, large variabilities exist in the actual irrigation efficiencies due to, e.g., farmers' management and maintenance of the system, the timing of irrigation, meteorological conditions during irrigation, and local topography (Benouniche et al., 2014). Differences between actual and pre-defined irrigation efficiency lead to a variability of irrigation estimates larger than one order of magnitude (Puy et al., 2022a). In addition, irrigation estimates from models are oftentimes inconsistent among different models, which might lead to misguided decisions (Puy et al., 2022b). A possible way to overcome some model limitations is offered by data assimilation techniques, which use (satellite) observations to constrain models (Reichle, 2008). Various studies explored the benefit of assimilating backscatter, brightness temperature, or soil moisture, for improving modelled soil moisture estimates (De Lannoy et al., 2022; De Lannoy and Reichle, 2016; Heyvaert et al., 2023), but further efforts are needed to better integrate models and observations when the goal is the retrieval of irrigation water amounts (Kumar et al., 2015; Modanesi et al., 2022).

Remotely sensed observations of hydrological variables that are proxies of irrigation, as for instance soil moisture, vegetation production, and land surface temperature, offer another opportunity do derive irrigation. In fact, remote sensing enables consistent monitoring of the Earth surface, providing spatially detailed and temporally continuous observations. A complete overview of how different satellite data can be used to estimate irrigation is given in Massari et al. (2021). Soil moisture, being directly linked to irrigation through the induced increase in soil water content, is suited to retrieve irrigation, as demonstrated with synthetic experiments and through the analysis of in-situ measurements (Brocca et al., 2018; Filippucci et al., 2020; Zappa et al., 2022). In particular, two irrigation retrieval algorithms based on satellite soil moisture information have been developed in recent years: the SM_Delta (Zappa et al., 2022, 2021; Zaussinger et al., 2019; Zohaib and Choi, 2020) and the SM_Inversion (Brocca et al., 2018; Dari et al., 2023, 2022, 2020; Jalilvand et al., 2019; Zhang et al., 2022) methods. In the SM_Delta approach, irrigation was originally conceived as the difference between satellite and modelled soil moisture data at coarse-resolution ($>$ 10 km), assuming that satellite observations contain (at least partially) irrigation-related signals, while modelled soil moisture based on meteorological forcing only does not (Zaussinger et al., 2019). More recently, the SM_Delta approach was revised to meet the increasing availability of high-resolution ($\leq$ 1 km) satellite soil moisture observations, i.e., from Sentinel-1 (Zappa et al., 2021). In this adapted methodology, instead of considering modelled soil moisture as baseline, irrigation is derived as the soil moisture difference between an irrigated pixel and its surrounding area (Zappa et al., 2022).

Alternatively, the SM_Inversion approach is based on the inversion of the soil water balance equation, where the unknown quantity is set to the total amount of water entering the soil, i.e., over agricultural areas, precipitation plus irrigation. Then, irrigation is obtained by subtracting precipitation from the total amount of water entering the soil. The SM_Inversion approach has been used extensively, both with coarse- and high-resolution soil moisture products (Brocca et al., 2018; Dari et al., 2023, 2022, 2020; Jalilvand et al., 2019).

The two approaches represent the state-of-the-art of irrigation retrievals using remotely sensed soil moisture observations, and both have been validated against ground reference data. However, a direct comparison of irrigation estimates derived from the SM_Delta and SM_Inversion approaches has not been carried out yet. To increase confidence in the reliability of satellite-derived irrigation estimates, and promote their employment across various end-users, estimates obtained from different approaches should be consistent, especially when the input data is the same.

The objective of this work, therefore, is to fill this gap and i) assess the agreement between irrigation estimates derived from the SM_Delta and SM_Inversion approaches and forced with the same input data, ii) explore the features of the irrigation estimates in terms of spatial patterns, temporal dynamics, and specific characteristics (e.g., number of irrigation events per year, average irrigation water amount per event) depending on irrigation system and crop type, and finally iii) identify strengths and limitations of each irrigation retrieval approach. Both methods have been applied over the Ebro basin, an extensively irrigation region in Spain, and are based on soil moisture derived from Sentinel-1 using the RT1 (first-order radiative transfer) model (Quast et al., 2023). The analysis is further complemented by considering a modelled approach, in order to assess the added value of satellite-based irrigation retrievals. In particular, model-only simulations by based on the configurations from Modanesi et al. (2022b), (2021) obtained with the Noah-MP land surface model (Noah-MP LSM; Niu et al., 2011), coupled to a sprinkler irrigation scheme (Ozdogan et al., 2010) are used as an independent irrigation dataset.

2. Data and Methods

2.1. Study area

Our analysis is carried out over the Ebro basin, located in north-east Spain (Fig. 1). The Ebro basin covers an area of approximately 83000 km^2 and is characterized by contrasting topography, ranging from the Cantabrian range and the Pyrenees in the north (up to 3000 m a.s.l.) to the flat Ebro river valley in the central part of the basin (López-Moreno et al., 2011). Consequently, a large spread in meteorological conditions is found within the basin, with precipitation varying between 300 and 2450 mm/year and annual average temperature ranging between 1 and 16 °C (López-Moreno et al., 2008). The abundance of water in mountainous areas has driven the construction of dams and regulation of the main rivers in order to serve hydropower production and irrigation (López-Moreno et al., 2002). Irrigated agriculture covers roughly 10% of the total area of the Ebro (Isidoro and Aragüés, 2007) and consumes up to 90% of the water resources in the basin (Quiroga et al., 2011). The most common crops cultivated in the Ebro are summer (mostly alfalfa and maize) and winter (mostly cereals) crops, followed by fruit trees, vegetables and vineyards (Quiroga et al., 2011; Salvador et al., 2011). Two additional datasets covering the entire Ebro basin are employed: i) a map classifying the irrigation systems in the Ebro basin (drip, sprinkler, and flood) available at 1 km resolution (LIAISE-Ebro-Methods-Irrigation-1 km, LE-MI-1, Barella-Ortiz et al., 2022), and ii) the EUCROP2018 dataset (d'Andrimont et al., 2021), also available for 2018 at 10 m resolution. The latter was upscaled to match the spatial resolution of the irrigation datasets using the mode, i.e., most common crop, after classifying as summer, winter, and permanent crops.

2.2. Reference data

Irrigation water amounts applied at the district level are available for four irrigated districts over the period 2017–2019 (Fig. 1, right). Together, the four irrigation districts cover an area of approximately 2100 km^2. The Urgell (URG) is predominantly irrigated with flood irrigation, while the Algerri Balaguer (AB) is characterized by extensive use of drip and sprinkler irrigation. In the North- and South- Catalan Aragonese districts (NCA and SCA) all three irrigation systems coexist, with sprinkler being the most common method (Dari et al., 2021; Paolini et al., 2022). In the study area, drip irrigation systems are often associated with permanent crops (orchards, vineyards, and olive trees), whereas sprinkler and flood irrigation are employed for winter cereals and summer crops (Paolini et al., 2022). A total of 11 annual benchmark irrigation time series are available, obtained from the four disctricts and the 3 years and after disregarding data for the AB district in 2018 because of a long data gap (> 80 days) during the irrigation period. It is worth noting that the benchmark irrigation water amounts were obtained dividing the daily volumes of water flowing through the irrigation channels (http://www.saihebro.com/saihebro/index.php?url=/datos/canales) by the area of each district, as in Dari et al. (2020). After visual inspection of the daily irrigation reference time series, they were smoothed using a rolling average of 21 days in order to reduce the impact of suspicious observations. Note that the subsequent comparisons against satellite-based irrigation estimates are conducted considering 15-daily, monthly, and yearly cumulative values, hence the impact of smoothing the reference time series is negligible (Supplement Figure S1).

2.3. Irrigation estimates

2.3.1. Satellite-based

Both irrigation retrievals are based on a Sentinel-1 surface soil moisture (S1-SSM) product obtained with a first-order radiative transfer model (RT1) (Quast et al., 2023). First, S1 backscatter is resampled to 1 km resolution to reduce noise and speckle effects, then soil moisture is retrieved in relative terms, i.e., degree of saturation. Satellite-based irrigation estimates have been retrieved over all agricultural pixels within the Ebro basin, according to Corine Land Cover 2018 (CLC 2018). The period under investigation consists of three full years, from January 2017 to December 2019.

The S1-SSM dataset showed good agreement with ERA5-Land top-layer soil moisture (Pearson R of 0.6) and has been successfully employed for the estimation of rainfall through the SM2RAIN algorithm (Filippucci et al., 2022). However, it should be highlighted that due to the mission observation scenario, i.e., partial overlap of some orbits, certain regions are observed more frequently than others (Figure S3) (Bauer-Marschallinger et al., 2019; Quast et al., 2023).

- SM_Delta

  The SM_Delta approach was initially developed to derive irrigation water use from coarse-resolution satellite products (Zaussinger et al., 2019). In particular, irrigation is calculated as the difference between satellite and modelled soil moisture forced with meteorological data only, under the assumption that satellite observations contain irrigation signals which are not present in the modelled soil moisture. Later, the method was adapted for handling high-resolution (≤ 1 km) satellite soil moisture products, i.e., from Sentinel-1 (Zappa et al., 2021). In the SM_Delta approach, S1-SSM is first converted to volumetric units multiplying it by the soil porosity derived from SoilGrids (Hengl et al., 2017), as in Zappa et al. (2021), and to the water column depth [mm] assuming a soil depth of 5 cm (Zaussinger et al., 2019). The updated version of the SM_Delta approach allows to calculate irrigation as the soil moisture difference between irrigated and surrounding rainfed fields (Zappa et al., 2022). Assuming that over a relatively small region, i.e., < 25 km

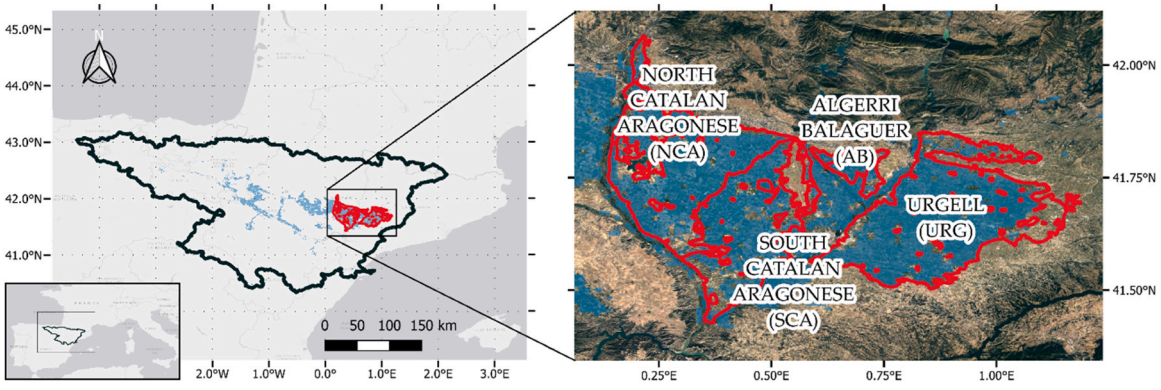

Fig. 1. Location of the Ebro basin in north-east Spain (left) and zoom in the four irrigation districts (right). Blue pixels in the background depict irrigated pixels according to an irrigation map specifically developed for the Ebro basin, i.e., LE-MI-1.

radius around an irrigated pixel, the meteorological forcing (precipitation and temperature) is consistent, the soil water balance of irrigated (Eq. 1) and rainfed fields (Eq. 2) between two consecutive satellite acquisitions can be described as follows:

$$d\theta_{irrig}/dt = Irr(t) + P(t) - g(t) - sr(t) - ET(t) \quad (1)$$

$$d\theta_{rainfed}/dt = P(t) - g(t) - sr(t) - ET(t) \quad (2)$$

where $d\theta/dt$ refers to the soil moisture change, expressed in mm, between two satellite acquisitions. Irr and P are irrigation and precipitation, g, sr, and ET depict drainage, surface runoff, and evapotranspiration [mm/day], respectively. The rainfed soil moisture is obtained as the average soil moisture of the S1-SSM pixels around the irrigated pixel within a 50 ×50 km grid. An additional requirement of the SM_Delta method is that over the surrounding region most fields are not irrigated simultaneously. The size of the surrounding window is selected to ensure a good balance between i) the assumption that meteorological conditions are homogeneous, and ii) the number of pixels used in the averaging. In fact, only surrounding pixels classified as cropland and with NDVI values similar (± 25%) to the irrigated pixel are considered to minimize potential differences arising from factors other than soil moisture, e.g., vegetation water content and structure (El Hajj et al., 2018, 2017).

Based on irrigated and rainfed soil moisture time series, each observation is flagged either as an irrigation or non-irrigation event. In particular, irrigation is detected when an irrigated pixel is characterized by a soil moisture difference between two consecutive acquisitions ($d\theta_{irrig}/dt$) larger than the difference found for the surrounding rainfed pixels ($d\theta_{rainfed}/dt$). Based on previous sensitivity analysis to account for noise in the data, we employ the following constraint for the detection of irrigation: $d\theta_{irrig}/dt > 1.01 * d\theta_{rainfed}/dt$ (Zappa et al., 2021). When the temporal gap between two satellite acquisitions is longer than 5 days, we conservatively disregard potential irrigation events as the soil moisture observations do not allow to effectively capture the irrigation-induced wetting and subsequent drying of the soil (Filippucci et al., 2020).

For the timestamps in which irrigation was detected, irrigation would be obtained as the absolute soil moisture difference between irrigated and rainfed pixels. It is implied that, except for irrigation, the other terms of the water balance in Eq.1 and Eq.2 are identical. However, several studies showed that ET can differ considerably between irrigated and rainfed fields (Brombacher et al., 2022; van Eekelen et al., 2015). If not accounted for, differences between irrigated and rainfed ET can lead to underestimations of irrigation (Kragh et al., 2023). Therefore, as suggested in Zappa et al. (2022b), we modify the irrigation retrieval by accounting not only for differences in soil moisture, but also for differences in ET between irrigated and rainfed fields:

$$Irr = (d\theta_{irrig}/dt - d\theta_{rainfed}/dt) + (ET_{irrig} - ET_{rainfed}) \quad (3)$$

The ET terms in Eq. 3 refer to actual evaporation rates and are obtained by multiplying potential ET (PET) by a stress factor, S. PET is computed by GLEAM v3.5b (Global Land Evaporation Amsterdam Model) using the Priestley and Taylor equation (Miralles et al., 2011), and similarly to Martens et al. (2017), the stress factor S (Eq. 4) accounts for phenological (Eq. 5) and water availability (Eq. 6) constraints:

$$S = S_{veg} \cdot S_{water} \quad (4)$$

$$S_{veg} = \sqrt{\frac{LAI}{LAI_{max}}} \quad (5)$$

$$S_{water} = 1 - \left(\frac{SM_{max} - SM}{SM_{max} - SM_{min}}\right)^2 \quad (6)$$

Where LAI (Leaf Area Index) and SM represent the time-varying values, and LAI_{max}, SM_{max}, and SM_{min} the minimum and maximum values observed for each pixel throughout the entire period (2017–2019), respectively. For the LAI, we employed the Copernicus Global Land Service (CGLS) product (https://land.copernicus.eu/global/products/lai), while SM refers to the S1-SSM dataset. As we expect the water stress S_{water} to be negligible immediately after irrigation, actual ET is calculated as follows:

$$ET_{irrig} = PET \cdot S_{veg} \quad (7)$$

$$ET_{rainfed} = PET \cdot S \quad (8)$$

- SM_Inversion

The SM_Inversion method (Brocca et al., 2018b) relies on the inversion of the satellite soil moisture signal for backward estimating the total amount of water entering the soil, which, over irrigated areas, is determined by the sum of rainfall plus irrigation. The potential of the approach was firstly tested with coarse resolution data (Brocca et al., 2018a; Jalilvand et al., 2019; Koster et al., 2016). Later on, the method was further refined and implemented with high-resolution data (Dari et al., 2022, 2020); recently, Dari et al. (2023) used the SM-based inversion approach to produce the first ever regional-scale high--resolution irrigation water use data sets over three major anthropized basins: the Ebro basin (Spain), the Po valley (Italy), and the Murray-Darling basin (Australia). The method relies on the inversion of the soil water balance, expressed as follows:

$$Z^* dSM(t)/dt = Irr(t) + P(t) - g(t) - sr(t) - ET(t) \quad (9)$$

in which Z* [mm] represents the soil water capacity, and SM(t) is the soil moisture expressed as saturation degrees. Consistently with Eq. 1, the remaining terms represent irrigation, precipitation, drainage, surface runoff and evaporation rates [mm/day]. Assuming $sr(t)$ to be negligible (Brocca et al., 2015), Eq. 9 can be rewritten as follows:

$$W_{in}(t) = Z^* dSM(t)/dt + a \cdot SM(t)^b + F \cdot SM(t) \cdot PET(t) \quad (10)$$

where $W_{in}(t)$ represents the sum of rainfall plus irrigation, the drainage term is expressed as $a \cdot SM(t)^b$, with a [mm] and b [-] representing drainage parameters (Famiglietti and Wood, 1994). The actual land evaporation rate is computed as the potential evaporation, $PET(t)$, multiplied by the available soil water content and corrected through an adjustment factor F ranging between 0.6 and 1.4. Details on the procedure for calibrating the algorithm's parameters a, b, Z^*, and F can be found in Dari et al. (2023). After computing the total amount of water entering into the soil, i.e., $W_{in}(t)$, the irrigation rates can be estimated by removing rainfall from the output, $Irr(t) = W_{in}(t) - P(t)$. Eventual negative irrigation rates are set to zero (Jalilvand et al., 2019) and negligible irrigation amounts due to random errors are disregarded by discarding results when the ratio between weekly estimated irrigation and weekly rainfall is lower than 0.2. Consistently with the data employed in the SM_Delta approach, irrigation estimates over the Ebro basin considered in this study rely on the S1-SSM product retrieved from the RT1 model and potential evaporation from GLEAM v3.5b (Martens et al., 2017). Additionally, input data of rainfall is obtained from ERA5-Land (Muñoz-Sabater et al., 2021).

2.3.2. Model-based

The Noah-Multiparameterization (Noah-MP) Land Surface Model (LSM) version 3.6 (Niu et al., 2011) was selected to provide

deterministic irrigation simulations, which are used as an additional dataset to assess the potential of the satellite-based irrigation products.

The Noah-MP LSM parameterization followed the default recommended option provided in the LIS documentation (https://nasa-lis.github.io/LISF/, last access: 05 July 2023): model time step of 15 min and a daily output interval, considering a spatial resolution of 0.01°. The fifth generation atmospheric reanalysis European Center for Medium-Range Weather Forecasts (ECMWF) Reanalysis (ERA5) (Hersbach et al., 2020) was used to force the LSM. A model spin up was performed for the period January 2000 until December 2014, while the deterministic run started from January 2015.

The Noah-MP LSM was additionally coupled to the sprinkler irrigation scheme developed by Ozdogan et al. (2010) to provide irrigation estimates at daily time scale. The irrigation module adds water as pseudo-precipitation after checking three main conditions, at the model grid scale: (i) where croplands are located and the irrigated land fraction, (ii) the start and end of the growing season and (iii) the root-zone soil moisture conditions. The first aspect is controlled by two datasets: the first one is a static land cover map, being the 2015 CGLS land cover map (Buchhorn et al., 2020), reclassified from the original 23 classes to the 14 classes supported by LIS and regridded from 100 m to 1 km spatial resolution; the second is the Global Rainfed and Paddy Cropland (GRIPC) (Salmon et al., 2015) used as input to map the irrigation fractional area. The growing season was defined based on a user-defined threshold of simulated LAI (i.e., LAI > 1) as in Modanesi et al. (2022). Finally, the irrigation is applied when the root-zone soil moisture availability falls below a user-defined threshold, which has been set to 50% of the field capacity (FC) as in Ozdogan et al. (2010). For more details on the Noah-MP LSM parameterization the reader can refer to Modanesi et al. (2022), (2021). It should be noted that these irrigation simulations should be taken as poor first guesses that were not calibrated in any way.

2.4. Evaluation & inter-comparison

2.4.1. Regional-scale assessment: irrigation mapping

The objective of this analysis is to assess whether irrigation estimates from the SM_Delta and SM_Inversion methods can be used to discriminate irrigated from rainfed pixels. Both satellite-based irrigation retrievals are applied to all agricultural pixels within the Ebro basin, i.e., without relying on any irrigation map (unlike model simulations), hence resembling real-world applications where this information is generally not available.

In the basic configuration, we calculate yearly irrigation water amounts for each pixel, and if irrigation is larger than 0 mm/year, the pixel is classified as irrigated, otherwise (i.e., irrigation $= 0$ mm/year) the pixel is set as rainfed. To reduce the effect of noise and other artefacts, we also define various thresholds of minimum yearly irrigation, i.e., a pixel is set as irrigated if yearly irrigation is higher than a predefined threshold. In particular, we consider six exclusion thresholds (1%, 5%, 10%, 20%, 30% and 50%) based on all the agricultural pixels within the entire Ebro basin.

Using the LE-MI-1 irrigation map, we classify irrigated and rainfed pixels as true positives (TP, irrigation retrieved over an irrigated pixel), false positives (FP, irrigation retrieved over a rainfed pixel), true negatives (TN, no irrigation retrieved over a rainfed pixel), and false negatives (FN, no irrigation retrieved over an irrigated pixel). Finally, we quantify the mapping accuracy computing three common metrics: user's accuracy (UA), producer's accuracy (PA) and overall accuracy (OA), as shown in Eqs. 11–13.

$$UA = TP/(TP + FP) \tag{11}$$

$$PA = TP/(TP + FN) \tag{12}$$

$$OA = (TP + TN)/(TP + TN + FP + FN) \tag{13}$$

2.4.2. Assessment at the irrigation district level: timing and quantification

In-situ reference time series, as well as satellite-based (SM_Delta and SM_Inversion) and model-based (Noah-MP) irrigation estimates, are available over the four irrigation districts described in Section 2.1. Modelled irrigation is included in the following assessment and intercomparison to evaluate the added value of satellite-based irrigation retrievals compared to traditional demand-driven models. First, we quantify the overall agreement between estimated and reference irrigation, both on a yearly basis and at biweekly frequency, which is the ideal temporal window required by basin authorities and water managers (Massari et al., 2021). Hence, irrigation time series are resampled to 15-daily resolution and the cumulative irrigation water amounts are calculated. The analysis is carried out considering three complementary metrics describing the similarity between time series: Pearson correlation (Pearson R), bias, and unbiased root mean squared deviation (ubRMSD).

Then, we evaluate the agreement among satellite- and model-based irrigation estimates in time and space. In particular, i) we derive the month with highest irrigation for each irrigated pixel, as water resources managers would benefit from knowing the period during which most water is consumed, and ii) we assess to what degree spatial patterns of yearly cumulative irrigation correspond.

Finally, we consider two additional aspects that can serve as a further qualitative check, and at the same time offer insights into potential applications of these irrigation datasets. First, we determine specific features depending on the irrigation methodology employed (drip, sprinkler, and flood) by considering yearly total amount, number of irrigation events, and average irrigation amount per event. For this analysis, daily irrigation time series are used, and timestamps characterized by irrigation amounts larger than 1 mm are flagged as irrigation events. Second, we explore differences in the irrigation timing depending on the crop type (summer, winter, and permanent crops).

3. Results and discussion

3.1. Regional-scale assessment: irrigation mapping

Here, we assess to what degree the irrigation estimates from the SM_Delta and SM_Inversion algorithms can be used to map irrigated and rainfed pixels. Fig. 2 shows, as an example, the correctness of pixels classified as irrigated and rainfed over the Ebro basin for the year 2017, considering a 20% threshold, i.e., pixels with a total yearly irrigation below the 20% percentile of the entire basin are set to rainfed. Both datasets capture irrigation over actually irrigated pixels (true positives, dark green), however, it is evident that irrigation is retrieved over numerous rainfed fields too (false positives, dark red). The overdetection of irrigated pixels is less pronounced in the SM_Delta irrigation dataset, which is characterized by the presence of several true negatives, i.e., no irrigation retrieved over rainfed pixels (light green colour). The difference between the two satellite-based irrigation datasets lies in the fact that the SM_Delta approach is only dependent on the satellite soil moisture dataset, and irrigation is not retrieved if the soil moisture of surrounding pixels is consistently higher compared to the pixel under analysis. On the other hand, the SM_Inversion method retrieves water entering the soil (i.e., precipitation plus irrigation) over each pixel. Hence, the reliability of the irrigation estimates derived with the SM_Inversion approach depends not only on the quality of soil moisture but also on the precipitation dataset used. Gomis-Cebolla et al. (2023) recently showed that ERA5-Land precipitation, which is the input to the SM_Inversion algorithm, is characterized by underestimations over large portions of the Ebro basin, especially during summer months, which could cause an overestimation of irrigation.

A quantitative comparison (user-, producer-, and overall- accuracies) among the two datasets, considering different exclusion threshold values, is presented in Fig. 2c. Both datasets have the tendency to

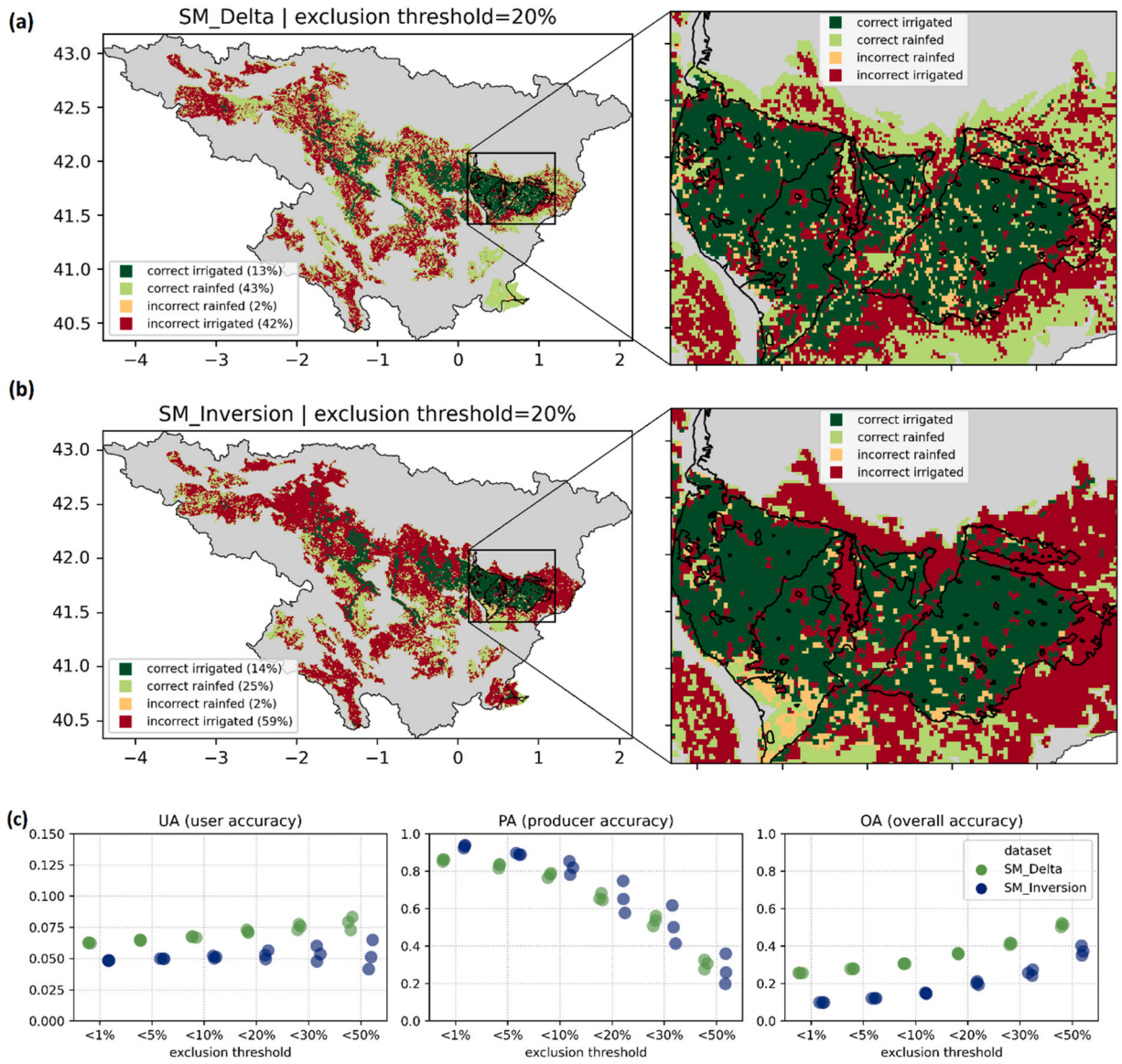

Fig. 2. Mapping accuracy obtained considering yearly irrigation estimates from the SM_Delta (panel a) and SM_Inversion (panel b) approaches over agricultural pixels only. Example maps showing correctly and incorrectly classified pixels over the entire Ebro basin and detail of the same data on the irrigated districts considering an exclusion threshold of 20%; summary of User-, Producer-, and Overall-accuracy (UA, PA, OA) obtained with various exclusion thresholds (c).

retrieve irrigation also over rainfed pixels, which leads to UA consistently lower than 0.1. The SM_Delta dataset achieves slightly better UA compared to SM_Inversion, while the SM_Inversion performs slightly better in terms of PA, i.e., a pixel classified as irrigated is actually irrigated. However, the PA decreases considerably by increasing the exclusion threshold, as more and more irrigated pixels are set to rainfed. The OA tends to increase with higher exclusion thresholds, because of the increasing number of true negatives, i.e., pixels set to rainfed because of low cumulative irrigation amounts. Nonetheless, PA scores show that raising the exclusion threshold leads to an increase of undetected pixels that are actually irrigated.

Overall, both SM_Delta and SM_Inversion approaches would substantially profit from being constrained by auxiliary maps of irrigated area, so that irrigation is not retrieved over rainfed pixels. To this end, spatially detailed (sub-field scale) and temporally dynamic (yearly) maps of irrigated areas would provide complementary information to the irrigation water amounts retrieved with the two approaches, enabling more reliable estimates. In the remainder of the manuscript, only actually irrigated pixels according to the LE-MI-1 map are considered, while rainfed pixels have been masked.

3.2. *Assessment at the irrigation district level: timing and quantification*

3.2.1. *District-scale dynamics*

Fig. 3 shows the temporal dynamics of reference and estimated irrigation over the four irrigated districts obtained from the SM_Delta (green) and SM_Inversion (blue) algorithms, as well as from the Noah-MP deterministic run (light brown). Note that irrigation time series are provided as 15-daily cumulative values. In addition, the agreement between yearly irrigation water amounts is displayed in the scatterplots on the right side of each panel.

Satellite-derived and model-based irrigation estimates are characterized by substantially different dynamics. Irrigation water amounts from Noah-MP are simulated over a shorter period due to model parameterization, i.e., a-priori determination of the irrigation season, and the amplitude is often larger compared to satellite-based estimates. Irrigation estimates from the SM_Delta and SM_Inversion approaches show rather similar dynamics, nonetheless, discrepancies in the

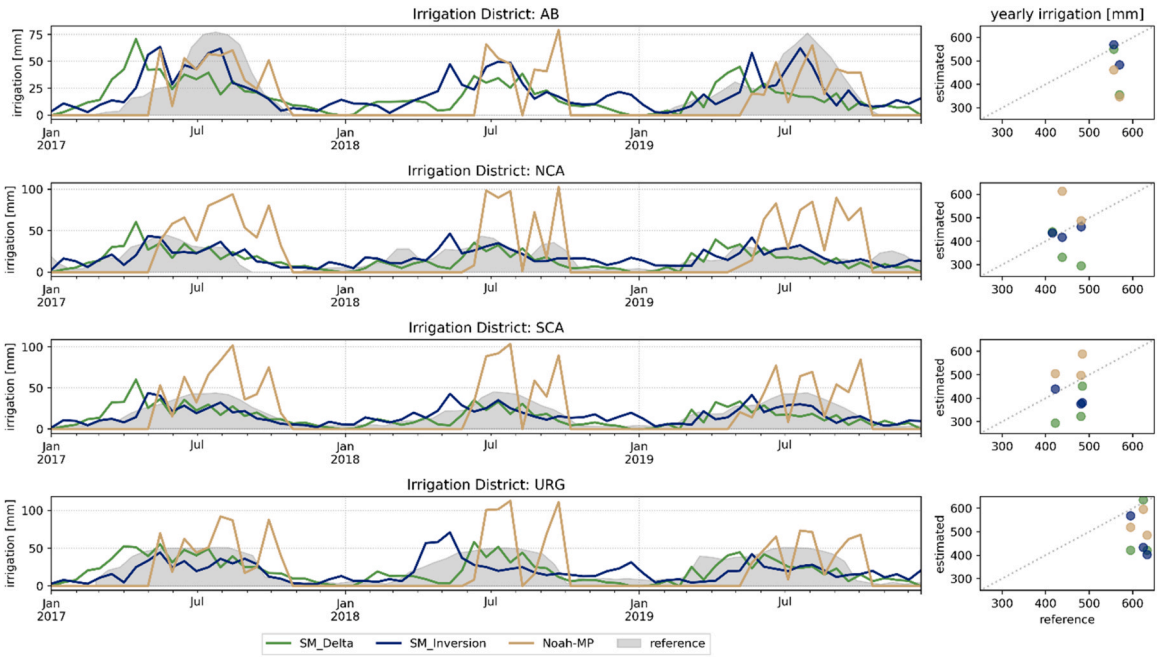

Fig. 3. Reference and estimated irrigation over the four irrigation districts: time series showing 15-daily cumulative irrigation (left) and scatterplots of yearly total irrigation (right). Note that the 2018 reference irrigation in the Algerri Balaguer (AB) district was excluded from further analysis because of a long data gap.

irrigation timing are found during spring months (April and May) in 2017 and 2018.

A possible explanation for this finding relies in the observational gaps lasting up to several days found in Sentinel-1 acquisitions in 2018. Within the SM_Delta approach, potential irrigation events are conservatively disregarded if two consecutive observations are separated by 5 days or more, while in the SM_Inversion approach these observations are included in the irrigation retrieval. This causes the lower irrigation observed in spring 2018 for the SM_Delta estimates.

When considering yearly water amounts, Noah-MP tends to overestimate irrigation in districts and years characterized by low irrigation supply and underestimate irrigation in years and districts associated with high irrigation amounts (Fig. 3, scatterplots). Satellite-based irrigation estimates can better capture the benchmark yearly water amounts, however, they are generally underestimating irrigation. This finding is consistent with the outcomes of previous studies, which highlighted that underestimations are expected when the spatial and/or temporal resolution of soil moisture observations are sub-optimal, i.e., pixel size larger than irrigated fields and/or revisit time longer than 1–2 days (Filippucci et al., 2020; Zappa et al., 2022).

We quantitatively assessed the agreement between reference and estimated irrigation time series considering 15-daily cumulative values in terms of Pearson R, bias, and ubRMSD (Fig. 4). On average, the three irrigation products achieve similar correlation values when evaluated against the benchmark irrigation (mean Pearson R around 0.7). Notably, both SM_Delta and SM_Inversion products are characterized by slightly negative biases (i.e., underestimate irrigation), in contrast to model-derived irrigation, and yielded considerably lower ubRMSD compared to Noah-MP estimates. Even though metrics from all three irrigation datasets fluctuate depending on the specific year and irrigation district considered, the satellite-based products are slightly more consistent across time and space compared to the model-based estimates. Overall, Fig. 4 suggests that satellite-derived irrigation can better represent actual irrigation dynamics, especially given that factors explaining (part of) such variability are well understood. As an example, the SM_Delta consistently shows low correlation and high ubRMSD values over the AB district. For context, more than 80% of the irrigated fields in the Algerri-Balaguer (AB) are equipped with drip irrigation, and it is known that monitoring irrigation from localized systems is more challenging (Zaussinger et al., 2019). Also, in most instances, both SM_Delta and SM_Inversion obtained lower negative biases (i.e., irrigation estimates closer to the reference data) in 2017 compared to other years. The explanation for this finding lies in the higher number of Sentinel-1 acquisitions during the main irrigation period, i.e., from March to September, in 2017 (84 acquisitions on average over the four districts) compared to 2018 and 2019 (70 and 65, respectively). Indeed, fewer soil

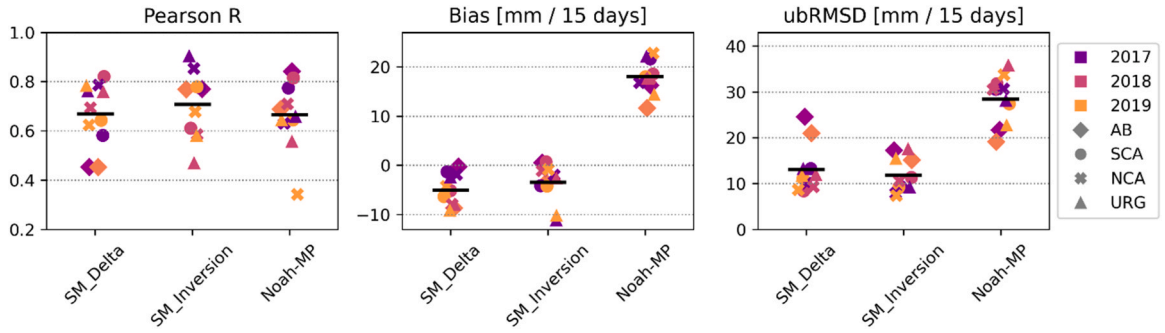

Fig. 4. Agreement between reference and estimated irrigation time series. Note that the evaluation metrics (Pearson R, bias, and ubRMSD) are calculated using 15-daily cumulative values. Results for individual districts and years can be identified, and the average values are shown with the black lines.

moisture observations are more likely to lead to undetected irrigation events, resulting in the subsequent underestimations of irrigation amounts (Zappa et al., 2022b).

3.2.2. Monthly irrigation peaks

Maps in Fig. 5 show the month with highest irrigation for the three products considered, as water resource managers are interested in the period during which most water is consumed. As reference irrigation data are only available at the district-scale, monthly time series are shown to allow a comparison with the irrigation estimates. It is evident that differences in spatial variability from Noah-MP irrigation estimates reflect underlying model input and parameters (e.g., soil properties), and the temporal component is driven by climatic conditions, i.e., precipitation and evaporation. On the other hand, both satellite-based products depict local, i.e., pixel-scale, differences in irrigation timing. However, limited agreement exists between the SM_Delta and SM_Inversion estimates in 2017 and, to a smaller extent in 2018. In fact, half of the pixels received most water between June and July 2017 according to the SM_Delta product, while almost 75% of the pixels were supplied the highest irrigation amounts in May based on the SM_Inversion. The consistency between the two satellite-derived irrigation estimates seems to be stronger in 2018, where the main differences concern irrigation

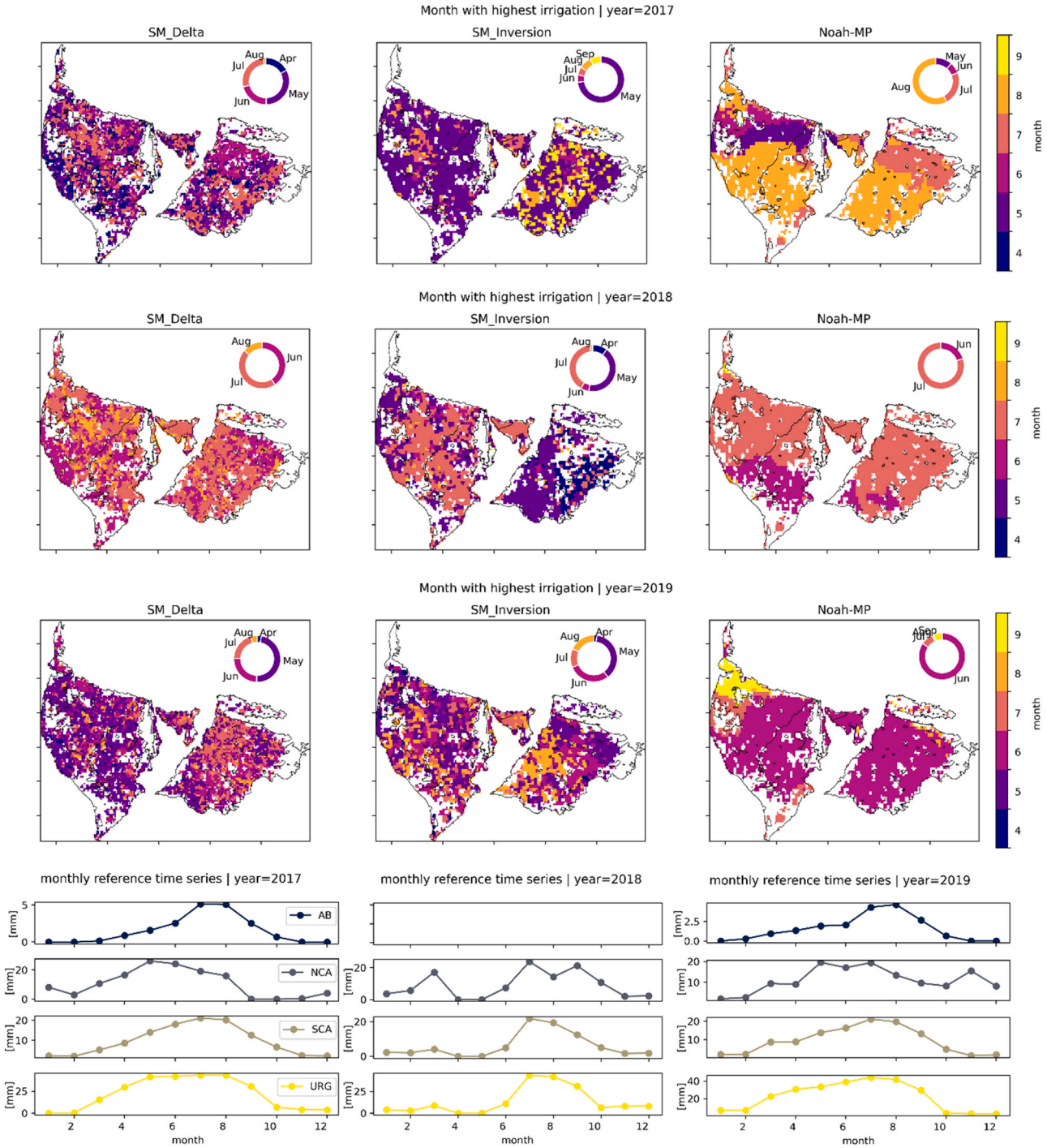

Fig. 5. Maps showing the month with the highest irrigation for each of the three years considered (2017–2019). The inset pie charts show the overall distribution of the irrigation peak months across the irrigated districts. District-scale reference irrigation time series are also shown for comparison.

peaks in the URG district, and, even more, in 2019. Also the spatial patterns, i.e., predominant month with highest irrigation, show moderate agreement, at least at the district scale. Overall, the timing of satellite-based irrigation peaks reflects relatively well the actual (district-scale) irrigation dynamics. Both SM_Delta and SM_Inversion estimates occasionally capture irrigation peaks earlier or later in the season compared to reference data, but the difference is generally no longer than one month.

Notably, the inter-annual variability of the irrigation peaks (as shown in the pie charts) derived from satellite-based estimates seems to be guided by meteorological conditions, hence the crop water requirements. The irrigation peaks occur earlier in 2017 and 2019 compared to 2018 according to both satellite-based approaches, with more pronounced differences in the SM_Delta estimates. Indeed, 2018 was characterized by heavy rainfall during April and May, which delayed the need for irrigation during the early stages of the growing season (as visible in the monthly irrigation reference time series, Fig. 5), while in 2017 and 2019 precipitation during the same months was considerably lower (Supplement Figure S2).

3.2.3. Spatial assessment

The spatial agreement among the three irrigation datasets is rather weak, with the highest spatial Pearson R between SM_Inversion and Noah-MP equal to 0.22 (Fig. 6). The consistency between yearly irrigation retrieved with the SM_Delta and SM_Inversion approaches is even lower, and the highest spatial correlation (0.12) between the two is obtained in 2017. Despite the rather low scores of spatial R referring to the entire irrigated districts area, a few consistent patterns can be observed between the SM_Delta and SM_Inversion yearly irrigation estimates. For instance, in 2017 both datasets portray lower irrigation in the southern part of the Urgell (URG) district, while the most heavily irrigated area is located in the Algerri Balaguer (AB) district, according to both satellite-based estimates. Such patterns are not reproduced by the Noah-MP irrigation estimates. Hence, despite the rather poor agreement obtained at the pixel-level, satellite-based estimates can still provide consistent spatial patterns when considering larger extents (e.g., district and regional scale).

Also, from Fig. 6 it is evident that the SM_Delta approach generally underestimates irrigation compared to SM_Inverison. Such discrepancies in amplitude can be explained by the specific model assumptions on soil water capacity employed in the two approaches. The soil water capacity is calculated multiplying the soil depth by the porosity, hence represents the amount of water that can be stored in a certain soil layer. In the SM_Delta approach, soil depth is fixed to 5 cm and soil porosity is derived from SoilGrids. The latter, i.e., soil porosity, roughly ranges between 40% and 43% over the irrigated districts, resulting in soil water capacity values of approximately 2 cm. In the SM_Inversion approach, soil water capacity is calibrated, and a median value of 7.9 cm was found over the Ebro basin, while lower values (approx. 5 cm) were obtained over the irrigated districts (Dari et al., 2023). As the soil water capacity directly affects the magnitude of the retrieved irrigation, i.e., higher values of soil water capacity leading to higher irrigation estimates, employing the same soil water capacity in both retrieval methods would largely reduce the differences in irrigation amplitude.

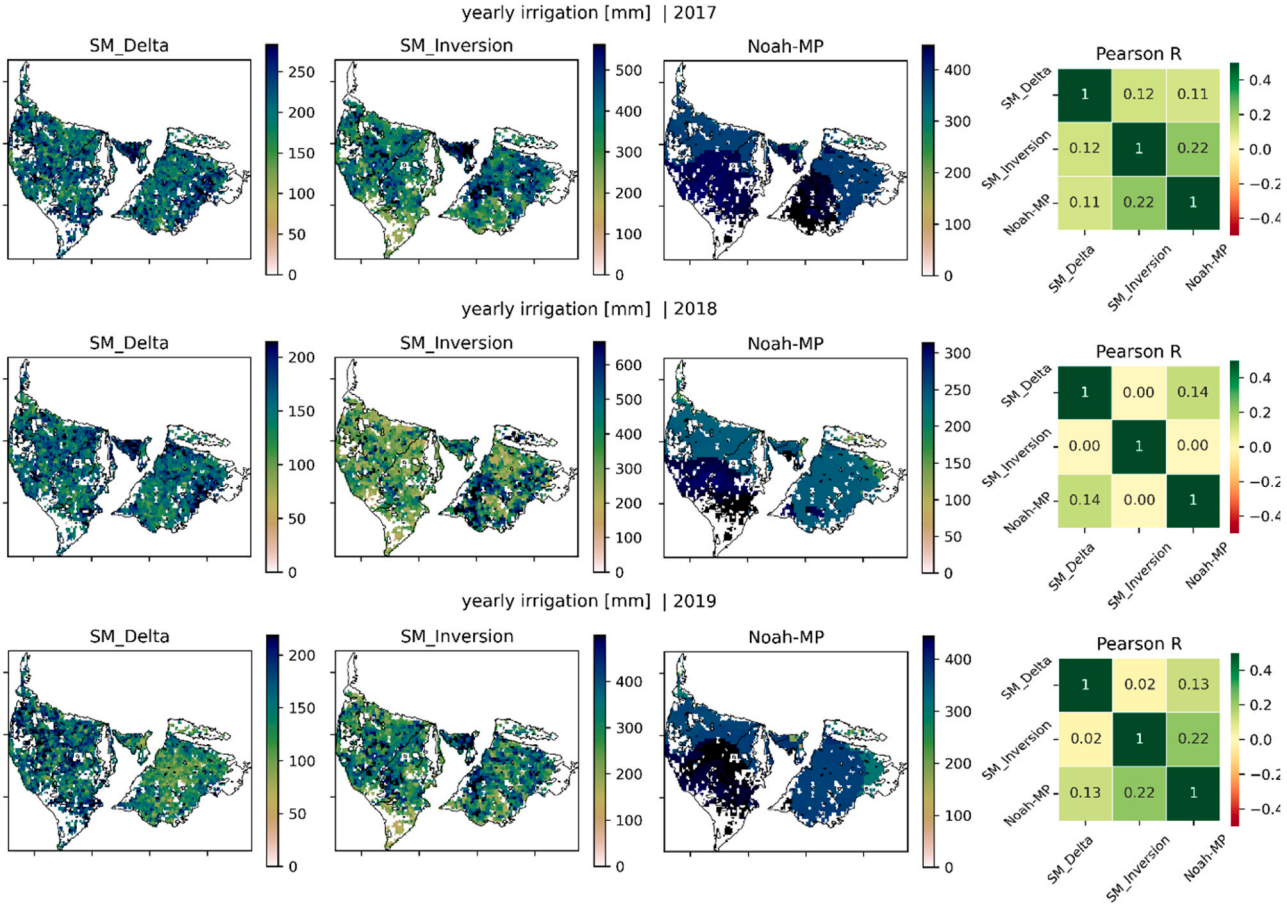

Fig. 6. Maps of yearly cumulated irrigation obtained from the SM_Delta and SM_Inversion approaches, and from Noah-MP. It should be noted that colorbars have different upper limits. The heat maps (panels on the right) depict the spatial correlation among the yearly irrigation obtained from the three methods.

3.3. Qualitative assessment and potential applications of irrigation datasets

In the following sections, we investigate two additional aspects that, on the one hand, serve as a qualitative check and assessment of the irrigation estimates, while at the same time showcase practical applications of such products. Note that, in this work, irrigation estimates derived from Noah-MP are based uniquely on a sprinkler irrigation scheme and do not discriminate between different crop types. However, because of the widespread lack of information on the type of irrigation system and the cultivated crops, modelled irrigation estimates are often retrieved with similar (sub-optimal) parameterization.

3.3.1. How much water is used by different irrigation systems?

Irrigation estimates from satellite soil moisture observations (SM_Delta and SM_Inversion approaches) and from a model (Noah-MP) are separated based on the irrigation system in place, i.e., drip, sprinkler, and flood. Details on the irrigation type within the Ebro basin are given in the LE-MI-1 irrigation map. The analysis aims at exploring potential differences in irrigation management and practices, total irrigation water amounts (Fig. 7a), number of irrigation events and average irrigation water amount applied at each irrigation event (Fig. 7b, c), depending on the irrigation system.

Overall, drip methods were found to provide the smallest contribution to the total irrigation occurring within the four irrigated districts, with consistent shares among the three datasets and years ranging between 11% and 15%. Estimates from the SM_Delta approach suggest a modest, but noticeable, shift from flood irrigation in favour of sprinkler systems over the period considered (contribution of flood irrigation to the total decreases from 41% to 36% between 2017 and 2019, while the share of sprinkler irrigation increases). Also, an overall reduction of the total amount of water supplied across the three years considered can be seen. This result, however, might be biased by the lower number of Sentinel-1 acquisitions in 2018 and 2019 compared to 2017. Also, the SM_Inversion-derived dataset portrays a drop of flood irrigation in 2019 compared to 2017, however, an increase in the fraction of flood irrigation is found in 2018 (42, 48, and 40% in 2017, 2018, and 2019, respectively). According to Noah-MP estimates, the relative contribution of the different irrigation systems to the total irrigation water volume varies only slightly across years: drip irrigation ranging between 12% and 14%, sprinkler systems accounting for 47–48%, and the remaining 38–40% ascribable to flood irrigation. We reiterate that, in this work, Noah-MP assumes that sprinkler irrigation is the only irrigation system in place over the region, and differences in the relative contribution from year to year are only caused by spatial differences in irrigation amounts over the different LE-MI-1 regions. For instance, in 2017 high irrigation water amounts were obtained over the AB district (see Fig. 6), where drip irrigation is widespread, resulting in a slightly higher relative contribution of drip irrigation in that year (Fig. 7a).

Additionally, we retrieved the average irrigation water amounts and the number of irrigation events for each pixel (Fig. 7b, c) to assess if differences between irrigation systems can be seen. The SM_Delta approach reproduces the diversity of irrigation practices associated with the system. Indeed, pixels irrigated with drip methods are characterized by lower amounts of water supplied more frequently compared to other systems. More water is generally applied during individual flood irrigation events, however, fewer irrigation events take place throughout the season. Pixels irrigated with sprinkler methods show intermediate characteristics. Irrigation estimates from the SM_Inversion yield contrasting outcomes: sprinkler irrigation is characterized by higher average water amounts, and flood events occur more frequently than irrigation under sprinkler and drip systems. It should be noted that the SM_Inversion approach assumes that surface runoff is negligible: while this is generally true over flat agricultural areas, it might be inaccurate when considering flood irrigation. Numerous fields in the URGELL district irrigated with flooding methods are in fact characterized by drainage systems that allow excess water to flow from one field to another. Hence, irrigation is likely underestimated for pixels characterized by flood irrigation, which is predominant in the URGELL. This finding is confirmed by Fig. 4, which shows that the largest underestimations from the SM_Inversion approach occur indeed in the URG district. Finally, model-based irrigation shows comparable values regardless of the irrigation system, as this information was not specified to the model.

It should be noted that differences, especially when considering the amount of water per irrigation event, are in general quite low (i.e., few mm of water). Nonetheless, the irrigation estimates account only for the water infiltrated in the soil, while other losses (due to, e.g., irrigation system and meteorological conditions) are not considered. Such losses could, however, increase the spread between the different irrigation

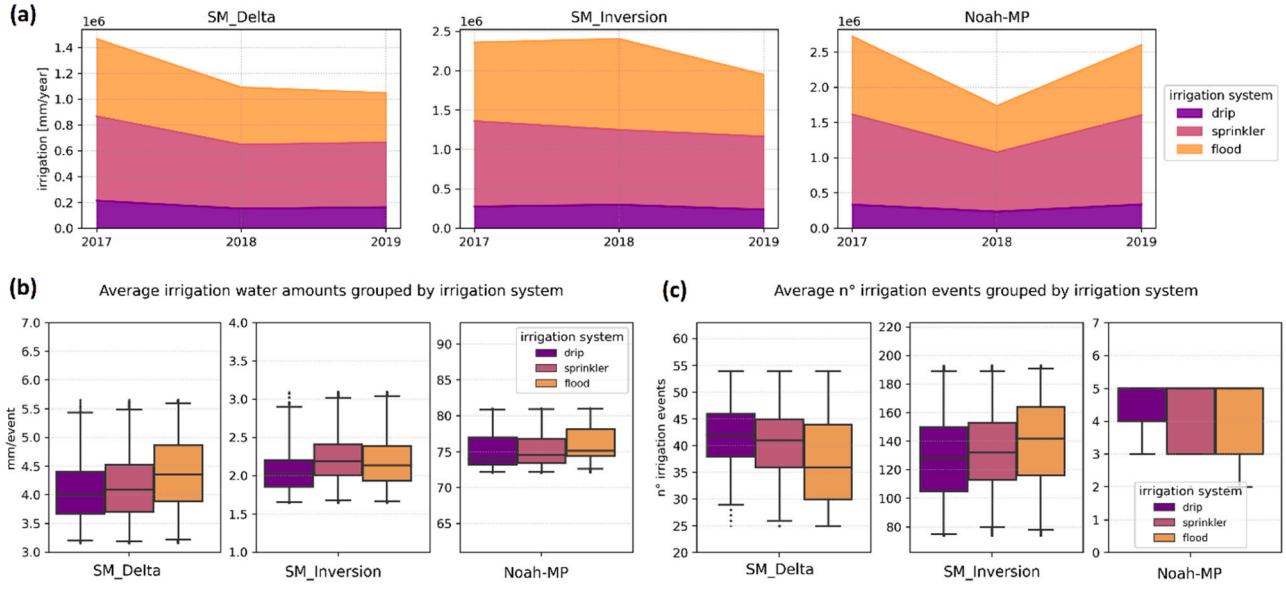

Fig. 7. Yearly irrigation water amounts associated with drip, sprinkler, and flood systems over the irrigated districts (a). Average irrigation water amounts supplied during each irrigation event (b), and number of irrigation events per pixel (c), grouped by irrigation system. LE-MI-1 irrigation map was used to separate satellite- and model- based irrigation estimates into pixels irrigated with drip, sprinkler, and flood systems.

systems (Dari et al., 2020).

3.3.2. How much water is used by different crop types?

Fig. 8a compares the monthly irrigation dynamics grouped for different crop types derived from EUCROP2018, namely winter, summer, and permanent crops. Again, this classification is not used neither in the satellite-based methods nor in Noah-MP, but we associate the estimated irrigation with the given crop map. Note that variations from the monthly average irrigation amounts are shown, i.e., a large positive (negative) value indicates that a big (small) share of the total monthly irrigation is directed towards a specific crop type. The two satellite-based irrigation estimates strongly agree, with large and positive (negative) irrigation water amounts during late spring and summer months for summer crops (winter crops). Irrigation over permanent crops is spread more evenly throughout the year, with small peaks in spring and autumn. It should be noted that a wide range of woody trees is classified as "permanent crops" umbrella, among which orchards, which are often irrigated in winter to prevent freezing. Clearly, each crop class is characterized by different water requirements across the year, depending on fruit development and ripening. Irrigation dynamics derived using Noah-MP are considerably different because the model does not use EUCROP2018, and assumes a summer crop everywhere. Consequently, permanent crops according to EUCROP2018 are extensively irrigated during summer months, while the relative contribution of irrigated summer crops is small (hence negative values) during summer.

In terms of irrigation water amounts per event (Fig. 8b) and per year (Fig. 8c), the SM_Delta and SM_Inversion approaches yield similar patterns, with higher (lower) values for summer crops (winter crops). Nonetheless, the overall amplitude of yearly irrigation water amounts is considerably different, with large underestimations obtained from the SM_Delta approach compared to SM_Inversion. Conversely, model-based irrigation estimates are characterized by similar amounts per event, as the irrigation scheme is based only on soil moisture but does not account for specific crop requirements.

4. Conclusions

Over the past couple of years, the SM_Delta and SM_Inversion approaches have been developed to retrieve irrigation water amounts from satellite soil moisture observed at high spatial resolution. Even if both methods have been tested and validated independently, a direct comparison among irrigation estimates from the two approaches has not been carried out yet. In this work, we performed a thorough intercomparison against reference irrigation data and assessed the consistency of irrigation estimates from the SM_Delta and SM_Inversion methods over an extensively irrigated region in Spain. Irrigation estimates from a Noah-MP land surface model deterministic run were also included as baseline, even if they only consider sprinkler irrigation and no prior information on the cultivated crop types.

The results revealed that irrigation retrieved from satellite soil moisture, using both the SM_Delta and SM_Inversion approaches, shows a better agreement with reference data compared to Noah-MP irrigation estimates. This finding emphasizes the need of providing reliable data constraints (e.g., maps of actually irrigated fields, crop types, and irrigation systems) to improve the realism of irrigation estimates produced by models. At the pixel-scale, irrigation estimates from the SM_Delta and SM_Inversion approaches showed limited consistency, which we could attribute to various factors in the retrieval algorithms. Discrepancies in irrigation were caused by differences in the estimation of soil water capacity and the assumption of negligible surface runoff made in the SM_Inversion method. Nonetheless, when aggregated in space or time, irrigation estimates from SM_Delta and SM_Inversion yielded consistent dynamics and patterns. For instance, estimates from both approaches capture the delayed irrigation occurred in 2018, compared to 2017 and 2019, due to the wetter conditions of spring 2018. Furthermore, the different irrigation timing between winter and summer crops was correctly captured by the SM_Delta and SM_Inversion irrigation estimates.

Overall, the study demonstrates the potential of employing high-resolution satellite soil moisture for the retrieval of irrigation information. Despite uncertainties in the irrigation estimates due to i) methodological formulations and assumptions, ii) quality and reliability of the input data (e.g., spatial resolution, revisit time, noise level), the two retrieval algorithms provided consistent results when transitioning from small- and short-scales (pixel level, sub-weekly) to larger- and longer-scales (district level, seasonal). Hence, remotely sensed irrigation estimates could inform policy makers, e.g., water resources managers and basin authorities, and can be beneficial to the modelling community by offering reliable constraints on the timing and the amounts of water

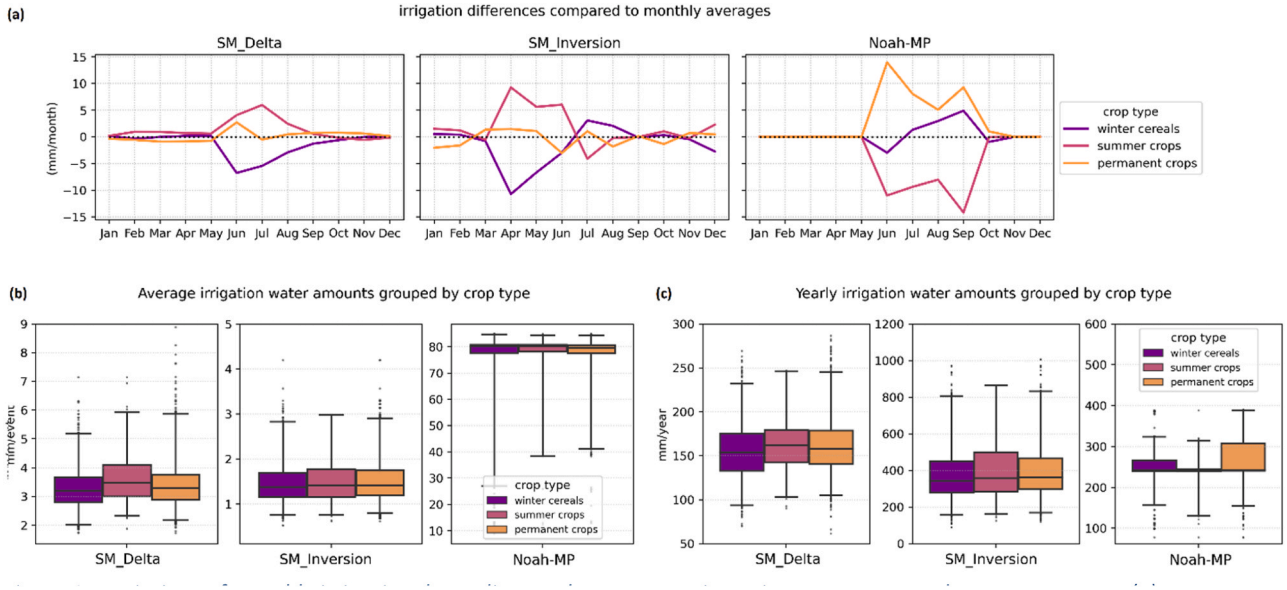

Fig. 8. Deviations of monthly irrigation depending on the crop type, i.e., winter, summer, and permanent crops (a). Large, positive values indicate larger contributions to the total irrigation. Average irrigation water amounts supplied during each irrigation event (b), and yearly irrigation water amounts (c), stratified by crop type.

employed at the basin level.

CRediT authorship contribution statement

De Lannoy Gabrielle: Funding acquisition, Writing – review & editing. **Massari Christian:** Funding acquisition, Writing – review & editing. **Dorigo Wouter:** Funding acquisition, Project administration, Supervision, Writing – review & editing. **Quintana-Seguí Pere:** Data curation, Validation, Writing – review & editing. **Barella-Ortiz Anais:** Data curation, Writing – review & editing. **Modanesi Sara:** Validation, Writing – review & editing, Data curation, Methodology. **Quast Raphael:** Data curation, Writing – review & editing. **Zappa Luca:** Conceptualization, Formal analysis, Methodology, Software, Validation, Visualization, Writing – original draft, Writing – review & editing. **Dari Jacopo:** Data curation, Methodology, Validation, Writing – review & editing. **Brocca Luca:** Funding acquisition, Writing – review & editing.

Declaration of Competing Interest

The authors declare that they have no known competing financial interests or personal relationships that could have appeared to influence the work reported in this paper.

Data availability

Data will be made available on request.

Acknowledgements

This research was funded by the European Space Agency through the projects IRRIGATION+ (contract number 4000129870/20/I-NB), 4DMED-Hydrology (contract number 4000136272/21/I-EF), and NEOMI (contract number 4000139242/22/NL/SD). The Noah-MP simulations were performed on the HPC of the Vlaams SuperComputer Center (VSC), supported by the Research Foundation Flanders (FWO) and C1 KU Leuven (C14/21/057). This study was partly supported by the IDEWA project (AEI PCI2020-112043) of the Partnership for research and innovation in the Mediterranean area (PRIMA). The authors acknowledge TU Wien Bibliothek for financial support through its Open Access Funding Programme.

Appendix A. Supporting information

Supplementary data associated with this article can be found in the online version at doi:10.1016/j.agwat.2024.108773.

References

Barella-Ortiz, A., Quintana-Segui, P., Dari, J., Brocca, L., Altés-Gaspar, V., Villar, J.M., Paolini, G., Escorihuela, M.J., Bonan, B., Calvet, J.-C., Tzanos, D., Munier, S., 2022. Simulation of irrigation in the Ebro River basin: new meteorological and physiographical datasets to better describe agriculture. Presented at the GESOC 2022: Colloque sur la Gestion de l'Eau en Zones Semi-arides, Outils, Changements globaux. https://doi.org/sciencesconf.org:gesoc2022:416020.

Bauer-Marschallinger, B., Freeman, V., Cao, S., Paulik, C., Schaufler, S., Stachl, T., Modanesi, S., Massari, C., Ciabatta, L., Brocca, L., Wagner, W., 2019. Toward global soil moisture monitoring with sentinel-1: harnessing assets and overcoming obstacles. IEEE Trans. Geosci. Remote Sens. 57, 520–539. https://doi.org/10.1109/TGRS.2018.2858004.

Benouniche, M., Kuper, M., Hammani, A., Boesveld, H., 2014. Making the user visible: analysing irrigation practices and farmers' logic to explain actual drip irrigation performance. Irrig. Sci. 32, 405–420. https://doi.org/10.1007/s00271-014-0438-0.

Brocca, L., Massari, C., Ciabatta, L., Moramarco, T., Penna, D., Zuecco, G., Pianezzola, L., Borga, M., Matgen, P., Martínez-Fernández, J., 2015. Rainfall estimation from in situ soil moisture observations at several sites in Europe: an evaluation of the SM2RAIN algorithm. J. Hydrol. Hydromech. 63, 201–209. https://doi.org/10.1515/johh-2015-0016.

Brocca, L., Tarpanelli, A., Filippucci, P., Dorigo, W., Zaussinger, F., Gruber, A., Fernández-Prieto, D., 2018a. How much water is used for irrigation? A new approach exploiting coarse resolution satellite soil moisture products. Int. J. Appl. Earth Obs. Geoinf. 73, 752–766. https://doi.org/10.1016/j.jag.2018.08.023.

Brocca, L., Tarpanelli, A., Filippucci, P., Dorigo, W., Zaussinger, F., Gruber, A., Fernández-Prieto, D., 2018b. How much water is used for irrigation? A new approach exploiting coarse resolution satellite soil moisture products. Int. J. Appl. Earth Obs. Geoinf. 73, 752–766. https://doi.org/10.1016/j.jag.2018.08.023.

Brombacher, J., Silva, I.R. de O., Degen, J., Pelgrum, H., 2022. A novel evapotranspiration based irrigation quantification method using the hydrological similar pixels algorithm. Agric. Water Manag. 267, 107602 https://doi.org/10.1016/j.agwat.2022.107602.

Buchhorn, M., Lesiv, M., Tsendbazar, N.-E., Herold, M., Bertels, L., Smets, B., 2020. Copernicus global land cover layers—Collection 2. Remote Sens. 12, 1044. https://doi.org/10.3390/rs12061044.

Cook, B.I., Shukla, S.P., Puma, M.J., Nazarenko, L.S., 2015. Irrigation as an historical climate forcing. Clim. Dyn. 44, 1715–1730. https://doi.org/10.1007/s00382-014-2204-7.

d'Andrimont, R., Verhegghen, A., Lemoine, G., Kempeneers, P., Meroni, M., Van Der Velde, M., 2021. From parcel to continental scale – A first European crop type map based on Sentinel-1 and LUCAS Copernicus in-situ observations. Remote Sens. Environ. 266, 112708 https://doi.org/10.1016/j.rse.2021.112708.

Dari, J., Brocca, L., Quintana-Seguí, P., Escorihuela, M.J., Stefan, V., Morbidelli, R., 2020a. Exploiting high-resolution remote sensing soil moisture to estimate irrigation water amounts over a Mediterranean Region. Remote Sens. 12, 2593. https://doi.org/10.3390/rs12162593.

Dari, J., Brocca, L., Quintana-Seguí, P., Escorihuela, M.J., Stefan, V., Morbidelli, R., 2020b. Exploiting high-resolution remote sensing soil moisture to estimate irrigation water amounts over a Mediterranean Region. Remote Sens. 12, 2593. https://doi.org/10.3390/rs12162593.

Dari, J., Quintana-Seguí, P., Escorihuela, M.J., Stefan, V., Brocca, L., Morbidelli, R., 2021. Detecting and mapping irrigated areas in a Mediterranean environment by using remote sensing soil moisture and a land surface model. J. Hydrol. 596, 126129 https://doi.org/10.1016/j.jhydrol.2021.126129.

Dari, J., Quintana-Seguí, P., Morbidelli, R., Saltalippi, C., Flammini, A., Giugliarelli, E., Escorihuela, M.J., Stefan, V., Brocca, L., 2022b. Irrigation estimates from space: Implementation of different approaches to model the evapotranspiration contribution within a soil-moisture-based inversion algorithm. Agric. Water Manag. 265, 107537 https://doi.org/10.1016/j.agwat.2022.107537.

Dari, J., Quintana-Seguí, P., Morbidelli, R., Saltalippi, C., Flammini, A., Giugliarelli, E., Escorihuela, M.J., Stefan, V., Brocca, L., 2022a. Irrigation estimates from space: implementation of different approaches to model the evapotranspiration contribution within a soil-moisture-based inversion algorithm. Agric. Water Manag. 265, 107537 https://doi.org/10.1016/j.agwat.2022.107537.

Dari, J., Brocca, L., Modanesi, S., Massari, C., Tarpanelli, A., Barbetta, S., Quast, R., Vreugdenhil, M., Freeman, V., Barella-Ortiz, A., Quintana-Seguí, P., Bretreger, D., Volden, E., 2023. Regional data sets of high-resolution (1 and 6 km) irrigation estimates from space. Earth Syst. Sci. Data 15, 1555–1575. https://doi.org/10.5194/essd-15-1555-2023.

De Lannoy, G.J.M., Reichle, R.H., 2016. Assimilation of SMOS brightness temperatures or soil moisture retrievals into a land surface model. Hydrol. Earth Syst. Sci. 20, 4895–4911. https://doi.org/10.5194/hess-20-4895-2016.

De Lannoy, G.J.M., Bechtold, M., Albergel, C., Brocca, L., Calvet, J.-C., Carrassi, A., Crow, W.T., De Rosnay, P., Durand, M., Forman, B., Geppert, G., Girotto, M., Hendricks Franssen, H.-J., Jonas, T., Kumar, S., Lievens, H., Lu, Y., Massari, C., Pauwels, V.R.N., Reichle, R.H., Steele-Dunne, S., 2022. Perspective on satellite-based land data assimilation to estimate water cycle components in an era of advanced data availability and model sophistication. Front. Water 4, 981745. https://doi.org/10.3389/frwa.2022.981745.

De Rosnay, P., 2003. Integrated parameterization of irrigation in the land surface model ORCHIDEE. Validation over Indian Peninsula. Geophys. Res. Lett. 30, 1986. https://doi.org/10.1029/2003GL018024.

Deng, J., Guo, L., Salas, W., Ingraham, P., Charrier-Klobas, J.G., Frolking, S., Li, C., 2018. Changes in irrigation practices likely mitigate nitrous oxide emissions from California Cropland. Glob. Biogeochem. Cycles 32, 1514–1527. https://doi.org/10.1029/2018GB005961.

Dorigo, W., Dietrich, S., Aires, F., Brocca, L., Carter, S., Cretaux, J.-F., Dunkerley, D., Enomoto, H., Forsberg, R., Güntner, A., Hegglin, M.I., Hollmann, R., Hurst, D.F., Johannessen, J.A., Kummerow, C., Lee, T., Luojus, K., Looser, U., Miralles, D.G., Pellet, V., Recknagel, T., Ruz Vargas, C., Schneider, U., Schoeneich, P., Schröder, M., Tapper, N., Vuglinsky, V., Wagner, W., Yu, L., Zappa, L., Zemp, M., Aich, V., 2021. Closing the water cycle from observations across scales: where do we stand? Bull. Am. Meteorol. Soc. 1–95. https://doi.org/10.1175/BAMS-D-19-0316.1.

van Eekelen, M.W., Bastiaanssen, W.G.M., Jarmain, C., Jackson, B., Ferreira, F., van der Zaag, P., Saraiva Okello, A., Bosch, J., Dye, P., Bastidas-Obando, E., Dost, R.J.J., Luxemburg, W.M.J., 2015. A novel approach to estimate direct and indirect water withdrawals from satellite measurements: A case study from the Incomati basin. Agric. Ecosyst. Environ. 200, 126–142. https://doi.org/10.1016/j.agee.2014.10.023.

El Hajj, M., Baghdadi, N., Zribi, M., Bazzi, H., 2017. Synergic Use of Sentinel-1 and Sentinel-2 Images for operational soil moisture mapping at high spatial resolution over agricultural areas. Remote Sens. 9, 1292. https://doi.org/10.3390/rs9121292.

El Hajj, M., Baghdadi, N., Bazzi, H., Zribi, M., 2018. Penetration analysis of SAR Signals in the C and L Bands for Wheat, Maize, and Grasslands. Remote Sens. 11, 31. https://doi.org/10.3390/rs11010031.

Famiglietti, J.S., 2014. The global groundwater crisis. Nat. Clim. Change 4, 945–948. https://doi.org/10.1038/nclimate2425.

Famiglietti, J.S., Wood, E.F., 1994. Multiscale modeling of spatially variable water and energy balance processes. Water Resour. Res. 30, 3061–3078. https://doi.org/10.1029/94WR01498.

Filippucci, P., Tarpanelli, A., Massari, C., Serafini, A., Strati, V., Alberi, M., Raptis, K.G. C., Mantovani, F., Brocca, L., 2020. Soil moisture as a potential variable for tracking and quantifying irrigation: a case study with proximal gamma-ray spectroscopy data. Adv. Water Resour. 136, 103502 https://doi.org/10.1016/j.advwatres.2019.103502.

Filippucci, P., Brocca, L., Quast, R., Ciabatta, L., Saltalippi, C., Wagner, W., Tarpanelli, A., 2022. High-resolution (1 km) satellite rainfall estimation from SM2RAIN applied to Sentinel-1: Po River basin as a case study. Hydrol. Earth Syst. Sci. 26, 2481–2497. https://doi.org/10.5194/hess-26-2481-2022.

Gomis-Cebolla, J., Rattayova, V., Salazar-Galán, S., Francés, F., 2023. Evaluation of ERA5 and ERA5-Land reanalysis precipitation datasets over Spain (1951–2020). Atmos. Res. 284, 106606 https://doi.org/10.1016/j.atmosres.2023.106606.

Hengl, T., Mendes de Jesus, J., Heuvelink, G.B.M., Ruiperez Gonzalez, M., Kilibarda, M., Blagotić, A., Shangguan, W., Wright, M.N., Geng, X., Bauer-Marschallinger, B., Guevara, M.A., Vargas, R., MacMillan, R.A., Batjes, N.H., Leenaars, J.G.B., Ribeiro, E., Wheeler, I., Mantel, S., Kempen, B., 2017. SoilGrids250m: Global gridded soil information based on machine learning. PLoS ONE 12, e0169748. https://doi.org/10.1371/journal.pone.0169748.

Hersbach, H., Bell, B., Berrisford, P., Hirahara, S., Horányi, A., Muñoz-Sabater, J., Nicolas, J., Peubey, C., Radu, R., Schepers, D., Simmons, A., Soci, C., Abdalla, S., Abellan, X., Balsamo, G., Bechtold, P., Biavati, G., Bidlot, J., Bonavita, M., Chiara, G., Dahlgren, P., Dee, D., Diamantakis, M., Dragani, R., Flemming, J., Forbes, R., Fuentes, M., Geer, A., Haimberger, L., Healy, S., Hogan, R.J., Hólm, E., Janisková, M., Keeley, S., Laloyaux, P., Lopez, P., Lupu, C., Radnoti, G., Rosnay, P., Rozum, I., Vamborg, F., Villaume, S., Thépaut, J., 2020. The ERA5 global reanalysis. Q. J. R. Meteorol. Soc. 146, 1999–2049. https://doi.org/10.1002/qj.3803.

Heyvaert, Z., Scherrer, S., Bechtold, M., Gruber, A., Dorigo, W., Kumar, S., De Lannoy, G., 2023. Impact of design factors for ESA CCI Satellite soil moisture data assimilation over Europe. J. Hydrometeorol. 24, 1193–1208. https://doi.org/10.1175/JHM-D-22-0141.1.

Isidoro, D., Aragüés, R., 2007. River water quality and irrigated agriculture in the Ebro Basin: an overview. Int. J. Water Resour. Dev. 23, 91–106. https://doi.org/10.1080/07900620601159743.

Jalilvand, E., Tajrishy, M., Ghazi Zadeh Hashemi, S.A., Brocca, L., 2019. Quantification of irrigation water using remote sensing of soil moisture in a semi-arid region. Remote Sens. Environ. 231, 111226 https://doi.org/10.1016/j.rse.2019.111226.

Koster, R.D., Brocca, L., Crow, W.T., Burgin, M.S., De Lannoy, G.J.M., 2016. Precipitation estimation using L-band and C-band soil moisture retrievals: precipitation estimation from soil moisture retrievals. Water Resour. Res. 52, 7213–7225. https://doi.org/10.1002/2016WR019024.

Kragh, S.J., Dari, J., Modanesi, S., Massari, C., Brocca, L., Fensholt, R., Stisen, S., Koch, J., 2023. An inter-comparison of approaches and frameworks to quantify irrigation from satellite data (preprint). Water Resour. Manag. /Remote Sens. GIS. https://doi.org/10.5194/hess-2023-142.

Kukal, M.S., Irmak, S., 2019. Irrigation-limited yield gaps: trends and variability in the United States post-1950. Environ. Res. Commun. 1, 061005 https://doi.org/10.1088/2515-7620/ab2aee.

Kumar, S.V., Peters-Lidard, C.D., Santanello, J.A., Reichle, R.H., Draper, C.S., Koster, R. D., Nearing, G., Jasinski, M.F., 2015. Evaluating the utility of satellite soil moisture retrievals over irrigated areas and the ability of land data assimilation methods to correct for unmodeled processes. Hydrol. Earth Syst. Sci. 19, 4463–4478. https://doi.org/10.5194/hess-19-4463-2015.

Lobell, D.B., Cassman, K.G., Field, C.B., 2009. Crop Yield Gaps: their importance, magnitudes, and causes. Annu. Rev. Environ. Resour. 34, 179–204. https://doi.org/10.1146/annurev.environ.041008.093740.

López-Moreno, J.I., Beguería, S., García-Ruiz, J.M., 2002. Influence of the Yesa reservoir on floods of the Aragón River, central Spanish Pyrenees. Hydrol. Earth Syst. Sci. 6, 753–762. https://doi.org/10.5194/hess-6-753-2002.

López-Moreno, J.I., Goyette, S., Beniston, M., 2008. Climate change prediction over complex areas: spatial variability of uncertainties and predictions over the Pyrenees from a set of regional climate models. Int. J. Climatol. 28, 1535–1550. https://doi.org/10.1002/joc.1645.

López-Moreno, J.I., Vicente-Serrano, S.M., Moran-Tejeda, E., Zabalza, J., Lorenzo-Lacruz, J., García-Ruiz, J.M., 2011. Impact of climate evolution and land use changes on water yield in the ebro basin. Hydrol. Earth Syst. Sci. 15, 311–322. https://doi.org/10.5194/hess-15-311-2011.

Martens, B., Miralles, D.G., Lievens, H., Van Der Schalie, R., De Jeu, R.A.M., Fernández-Prieto, D., Beck, H.E., Dorigo, W.A., Verhoest, N.E.C., 2017. GLEAM v3: satellite-based land evaporation and root-zone soil moisture. Geosci. Model Dev. 10, 1903–1925. https://doi.org/10.5194/gmd-10-1903-2017.

Massari, C., Modanesi, S., Dari, J., Gruber, A., De Lannoy, G.J.M., Girotto, M., Quintana-Seguí, P., Le Page, M., Jarlan, L., Zribi, M., Ouaadi, N., Vreugdenhil, M., Zappa, L., Dorigo, W., Wagner, W., Brombacher, J., Pelgrum, H., Jaquot, P., Freeman, V., Volden, E., Fernandez Prieto, D., Tarpanelli, A., Barbetta, S., Brocca, L., 2021. A review of irrigation information retrievals from space and their utility for users. Remote Sens. 13, 4112. https://doi.org/10.3390/rs13204112.

McDermid, S., Nocco, M., Lawston-Parker, P., Keune, J., Pokhrel, Y., Jain, M., Jägermeyr, J., Brocca, L., Massari, C., Jones, A.D., Vahmani, P., Thiery, W., Yao, Y., Bell, A., Chen, L., Dorigo, W., Hanasaki, N., Jasechko, S., Lo, M.-H., Mahmood, R., Mishra, V., Mueller, N.D., Niyogi, D., Rabin, S.S., Sloat, L., Wada, Y., Zappa, L., Chen, F., Cook, B.I., Kim, H., Lombardozzi, D., Polcher, J., Ryu, D., Santanello, J., Satoh, Y., Seneviratne, S., Singh, D., Yokohata, T., 2023. Irrigation in the Earth system. Nat. Rev. Earth Environ. https://doi.org/10.1038/s43017-023-00438-5.

Miralles, D.G., Holmes, T.R.H., De Jeu, R.A.M., Gash, J.H., Meesters, A.G.C.A., Dolman, A.J., 2011. Global land-surface evaporation estimated from satellite-based observations. Hydrol. Earth Syst. Sci. 15, 453–469. https://doi.org/10.5194/hess-15-453-2011.

Modanesi, S., Massari, C., Gruber, A., Lievens, H., Tarpanelli, A., Morbidelli, R., De Lannoy, G.J.M., 2021. Optimizing a backscatter forward operator using Sentinel-1 data over irrigated land. Hydrol. Earth Syst. Sci. 25, 6283–6307. https://doi.org/10.5194/hess-25-6283-2021.

Modanesi, S., Massari, C., Bechtold, M., Lievens, H., Tarpanelli, A., Brocca, L., Zappa, L., De Lannoy, G.J.M., 2022b. Challenges and benefits of quantifying irrigation through the assimilation of Sentinel-1 backscatter observations into Noah-MP. Hydrol. Earth Syst. Sci. 26, 4685–4706. https://doi.org/10.5194/hess-26-4685-2022.

Modanesi, S., Massari, C., Bechtold, M., Lievens, H., Tarpanelli, A., Brocca, L., Zappa, L., De Lannoy, G.J.M., 2022a. Challenges and benefits of quantifying irrigation through the assimilation of Sentinel-1 backscatter observations into Noah-MP. Hydrol. Earth Syst. Sci. 26, 4685–4706. https://doi.org/10.5194/hess-26-4685-2022.

Muñoz-Sabater, J., Dutra, E., Agustí-Panareda, A., Albergel, C., Arduini, G., Balsamo, G., Boussetta, S., Choulga, M., Harrigan, S., Hersbach, H., Martens, B., Miralles, D.G., Piles, M., Rodríguez-Fernández, N.J., Zsoter, E., Buontempo, C., Thépaut, J.-N., 2021. ERA5-Land: a state-of-the-art global reanalysis dataset for land applications. Earth Syst. Sci. Data 13, 4349–4383. https://doi.org/10.5194/essd-13-4349-2021.

Niu, G.-Y., Yang, Z.-L., Mitchell, K.E., Chen, F., Ek, M.B., Barlage, M., Kumar, A., Manning, K., Niyogi, D., Rosero, E., Tewari, M., Xia, Y., 2011. The community Noah land surface model with multiparameterization options (Noah-MP): 1. Model description and evaluation with local-scale measurements. J. Geophys. Res. 116, D12109 https://doi.org/10.1029/2010JD015139.

Ozdogan, M., Rodell, M., Beaudoing, H.K., Toll, D.L., 2010. Simulating the effects of irrigation over the United States in a land surface model based on satellite-derived agricultural data. J. Hydrometeorol. 11, 171–184. https://doi.org/10.1175/2009JHM1116.1.

Paolini, G., Escorihuela, M.J., Merlin, O., Sans, M.P., Bellvert, J., 2022. Classification of different irrigation systems at field scale using time-series of remote sensing data. IEEE J. Sel. Top. Appl. Earth Obs. Remote Sens. 15, 10055–10072. https://doi.org/10.1109/JSTARS.2022.3222884.

Pei, L., Moore, N., Zhong, S., Kendall, A.D., Gao, Z., Hyndman, D.W., 2016. Effects of irrigation on summer precipitation over the United States. J. Clim. 29, 3541–3558. https://doi.org/10.1175/JCLI-D-15-0337.1.

Pokhrel, Y., Hanasaki, N., Koirala, S., Cho, J., Yeh, P.J.-F., Kim, H., Kanae, S., Oki, T., 2012. Incorporating anthropogenic water regulation modules into a land surface model. J. Hydrometeorol. 13, 255–269. https://doi.org/10.1175/JHM-D-11-013.1.

Pokhrel, Y.N., Hanasaki, N., Wada, Y., Kim, H., 2016. Recent progresses in incorporating human land–water management into global land surface models toward their integration into Earth system models. WIREs Water 3, 548–574. https://doi.org/10.1002/wat2.1150.

Puy, A., Sheikholeslami, R., Gupta, H.V., Hall, J.W., Lankford, B., Lo Piano, S., Meier, J., Pappenberger, F., Porporato, A., Vico, G., Saltelli, A., 2022b. The delusive accuracy of global irrigation water withdrawal estimates. Nat. Commun. 13, 3183. https://doi.org/10.1038/s41467-022-30731-8.

Puy, A., Lankford, B., Meier, J., Van Der Kooij, S., Saltelli, A., 2022a. Large variations in global irrigation withdrawals caused by uncertain irrigation efficiencies. Environ. Res. Lett. 17, 044014 https://doi.org/10.1088/1748-9326/ac5768.

Quast, R., Wagner, W., Bauer-Marschallinger, B., Vreugdenhil, M., 2023. Soil moisture retrieval from Sentinel-1 using a first-order radiative transfer model—A case-study over the Po-Valley. Remote Sens. Environ. 295, 113651 https://doi.org/10.1016/j.rse.2023.113651.

Quiroga, S., Fernández-Haddad, Z., Iglesias, A., 2011. Crop yields response to water pressures in the Ebro basin in Spain: risk and water policy implications. Hydrol. Earth Syst. Sci. 15, 505–518. https://doi.org/10.5194/hess-15-505-2011.

Reichle, R.H., 2008. Data assimilation methods in the Earth sciences. Adv. Water Resour. 31, 1411–1418. https://doi.org/10.1016/j.advwatres.2008.01.001.

Salmon, J.M., Friedl, M.A., Frolking, S., Wisser, D., Douglas, E.M., 2015. Global rain-fed, irrigated, and paddy croplands: a new high resolution map derived from remote sensing, crop inventories and climate data. Int. J. Appl. Earth Obs. Geoinf. 38, 321–334. https://doi.org/10.1016/j.jag.2015.01.014.

Salvador, R., Martínez-Cob, A., Cavero, J., Playán, E., 2011. Seasonal on-farm irrigation performance in the Ebro basin (Spain): crops and irrigation systems. Agric. Water Manag. 98, 577–587. https://doi.org/10.1016/j.agwat.2010.10.003.

Siebert, S., Kummu, M., Porkka, M., Döll, P., Ramankutty, N., Scanlon, B., 2015. A global data set of the extent of irrigated land from 1900 to 2005. Hydrol. Earth Syst. Sci. https://doi.org/10.5194/hess-19-1521-2015.

Unesco (Ed.), 2019. Leaving no one behind, The United Nations world water development report. UNESCO, Paris.

Vogel, E., Donat, M.G., Alexander, L.V., Meinshausen, M., Ray, D.K., Karoly, D., Meinshausen, N., Frieler, K., 2019. The effects of climate extremes on global agricultural yields. Environ. Res. Lett. 14, 054010 https://doi.org/10.1088/1748-9326/ab154b.

Zappa, L., Schlaffer, S., Bauer-Marschallinger, B., Nendel, C., Zimmerman, B., Dorigo, W., 2021. Detection and quantification of irrigation water amounts at 500 m using sentinel-1 surface soil moisture. Remote Sens. 13, 1727. https://doi.org/10.3390/rs13091727.

Zappa, L., Schlaffer, S., Brocca, L., Vreugdenhil, M., Nendel, C., Dorigo, W., 2022a. How accurately can we retrieve irrigation timing and water amounts from (satellite) soil moisture? Int. J. Appl. Earth Obs. Geoinf. 113, 102979 https://doi.org/10.1016/j.jag.2022.102979.

Zaussinger, F., Dorigo, W., Gruber, A., Tarpanelli, A., Filippucci, P., Brocca, L., 2019. Estimating irrigation water use over the contiguous United States by combining

satellite and reanalysis soil moisture data. Hydrol. Earth Syst. Sci. 23, 897–923. https://doi.org/10.5194/hess-23-897-2019.
Zhang, K., Li, X., Zheng, D., Zhang, L., Zhu, G., 2022. Estimation of global irrigation water use by the integration of multiple satellite observations. Water Resour. Res. 58 https://doi.org/10.1029/2021WR030031.
Zohaib, M., Choi, M., 2020. Satellite-based global-scale irrigation water use and its contemporary trends. Sci. Total Environ. 714, 136719 https://doi.org/10.1016/j.scitotenv.2020.136719.